Journal of Materials Chemistry A

Accepted Manuscript

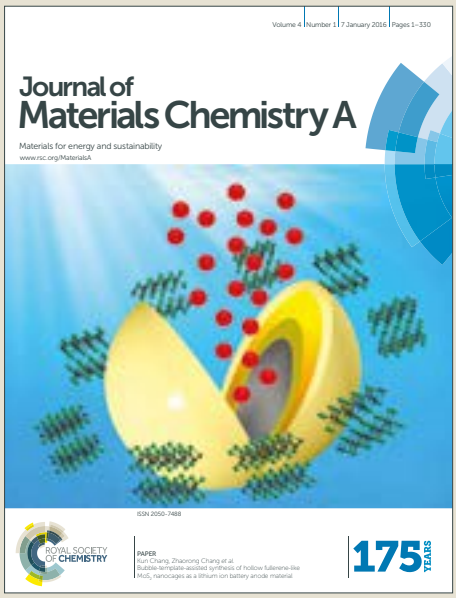

ROYAL SOCIETY OF CHEMISTRY

rsc.li/materials-a

View Article Online
DOI: 10.1039/C8TA02793E

Journal of Materials Chemistry A

ARTICLE

Layer-to-layer distance determines the performance of 3D bio-electrochemical lamellar anodes in microbial energy transduction processes

Received 00th January 20xx,
Accepted 00th January 20xx

DOI: 10.1039/x0xx00000x

www.rsc.org/

Diego Massazza,[a] Juan P. Busalmen, [a] Rodrigo Parra[b] and Hernán E. Romeo *[c]

Microbial fuel cells (MFCs) harness the metabolic machinery of electro-active bacteria to transfer electrons from organic molecules to polarized anodes. In this context, increasingly higher anode surface areas have been pursued for maximizing MFC performance. In this study we prepared 3D layered Ti_4O_7 electrodes with different interlayer spacing (from 10 to 100 µm) but mantaining the same total void fraction (90%), so as to modify the electrode surface-to-volume ratios. This allowed us to test the hypothesis that there must be a limit in surface area per unit volume restricting the efficiency of 3D porous bio-electrochemical anodes. The lamellar scaffolds were evaluated in three-electrode cells cultured with *G. sulfurreducens*. Regardless of electrode interlayer spacing or biofilm developmental stage, the electron transfer rate was constant (0.11 pA/bacterium), with current scaling linearly with the size of the microbial population. However, maximum volumetric current densities (20 ± 0.8 $kA.m^{-3}$) were not obtained from electrodes with maximum surface-to-volume ratios (shorter interlayer distances), because bacterial biomass was not directly paired to surface area. This demonstrated that, by controlling the spacing between layers, it is possible to modulate the amount of bacteria per electrode unit volume, this ratio determining the final electrode performance. The limit obtained in surface area suggested that other effects, as fluid dynamic constraints inside the "slit-shaped" pores, must be playing a critical role on anode performance.

Introduction

Aligned to the current pushing challenge of revaluating urban and industrial wastewaters, microbial electrochemical technologies (METs) have emerged to efficiently interconvert chemical and electrical energy.[1,2] Hand in hand with this approach, microbial energy conversion has been explored as an alternative way for transitioning to sustainable energy technologies.[3] In particular, microbial fuel cells (MFCs) have come up as promising devices to directly drive electrons from contaminating organic molecules to polarized anodes, by harnessing the metabolic routes of electro-active bacteria.[4-6] Theoretically, and provided they are equipped with perfect electrodes on which the bio-electrochemical reactions can proceed at "infinite" rates, ideal MFCs with negligible internal resistance and high Coulombic efficiency may convert the entire free energy associated to organics oxidation into electricity. While it is true that perfect electrodes are still utopic, recent efforts directed to obtain increasingly higher anodic volumetric current densities have produced a substantial progress via the introduction of highly structured 3D conducting scaffolds.[7-12] Obtained from different materials and following a variety of strategies, 3D open macroporous bio-anodes have been first claimed and then demonstrated to be the option of choice for substantially increasing the electrode surface-to-wastewater volume ratio, leading consequently to remarkable boosts in the ultimate MFC efficiency. However, the continuous pursuit of a better bio-anode performance has mainly walked towards increasingly higher surface areas per electrode unit volume, having not included a rational analysis of the porosity fragmentation (i.e., the way in which the effective electrode void fraction is distributed as pores of the same size, shape and morphology), an overlooked property of porous electrodes with paradigmatic value. In this way, while the total porosity of a 3D bio-anode can be kept constant, it is relevant to note that it can be strategically fragmented through the electrode volume conforming uniform pores of selected size and/or morphology. This should not be misinterpreted or confused with the concept of pore size distribution, as the latter refers to a range of pores of different size along the entire electrode volume.

[a] División Ingeniería de Interfaces y Bio-procesos, Instituto de Investigaciones en Ciencia y Tecnología de Materiales (INTEMA), Consejo Nacional de Investigaciones Científicas y Técnicas (CONICET), 7600, Mar del Plata, Argentina.
[b] División Cerámicos, Instituto de Investigaciones en Ciencia y Tecnología de Materiales (INTEMA), Consejo Nacional de Investigaciones Científicas y Técnicas (CONICET), 7600, Mar del Plata, Argentina.
[c] División Polímeros Nanoestructurados, Instituto de Investigaciones en Ciencia y Tecnología de Materiales (INTEMA), Consejo Nacional de Investigaciones Científicas y Técnicas (CONICET), 7600, Mar del Plata, Argentina.
E-mail: hromeo@fi.mdp.edu.ar

Electronic Supplementary Information (ESI) available: electrode processing conditions (Fig. S1), diagram of the experimental set up (Fig. S2), electrochemical determination of relative electrode surface areas (Fig. S3), SEM images of ITTC electrodes (Fig. S4), bio-electrochemical electrode performance as a function of interlayer distance (Fig. S5) and SEM characterization of *G. sulfurreducens* biofilms (Fig. S6). See DOI: 10.1039/x0xx00000x

View Article Online
DOI: 10.1039/C8TA02793E

According to the proposed approach, the total anode porosity can be uniformly fragmented by building up 3D layered electrodes, generating "slit-shaped" pores with controlled size. This allows modulating, by controlling the distance between the electrode layers (but maintaining the same total porosity), not only the effective surface area exposed to the electrolyte but also critical geometric parameters intimately linked to transport phenomena. This is particularly relevant in the design of structures intended to host live entities as, for instance, electro-active bacteria, offering them suitable living conditions.

In this study, we tested the hypothesis that there must be a limit in surface area per electrode unit volume restricting the efficiency of porous bio-anodes. For this, the effect of layer-to-layer distance of 3D lamellar anodes on bacterial energy conversion was assessed. The proof-of-concept involved the use of recently reported high-performance 3D ceramic bio-anodes built on the chemistry of electrically conducting titanium sub-oxides (Ti_4O_7),[7] in combination with *Geobacter sulfurreducens*, the most efficient electricity-producing bacteria ever reported.[13,14] The main feature of the electrodes used (termed ITTC, ice-templated titanium-based ceramics) is their ordered porosity, distributed as straight lamella-like channels running from one electrode end to the other. To prove the introduced concept, the electrode interlayer distances were tuned by changing the cryogenic mixture used in the electrode building-up process (see the Experimental Section and Fig. S1 in the Electronic Supplementary Information, ESI). This allowed assembling four electrode configurations, all of them characterized by a constant total porosity of 90%, but exhibiting (each of them) uniform layer-to-layer distances ranging from 10 µm to 100 µm. Accordingly, the approach yielded conducting scaffolds with different surface-to-volume ratios. This allowed finally testing the effect of the exposed surface area on the electrode efficiency.

In this study we demonstrate that maximum volumetric current densities were not obtained from electrodes with maximum surface-to-volume ratios, because bacterial biomass was not directly paired to surface area. Accordingly, by controlling the spacing between the electrode layers, it is possible to modulate the amount of bacteria per electrode unit volume, which finally determines the electrode performance. The presented findings demonstrate that the limit obtained in surface area might be ascribed to fluid dynamic constraints inside the "slit-shaped" pores, which must be playing a critical role on transport phenomena affecting the electro-active bacteria confined in the porous bio-electrochemical anodes.

Experimental

Preparation of ITTC bio-anodes

Porous supports were prepared from TiO_2 aqueous dispersions via directional freezing, according to previously reported protocols.[7] Briefly, dispersions were poured into plastic moulds and were vertically dipped at a controlled constant rate into a cold bath, to induce the orientation of the growing lamellar ice crystals. In order to modulate the interlayer spacing in each sample, different immersion rates and cooling liquids were used. According to the master curves shown in Fig. S1 (ESI), four layer-to-layer distances were produced in each scaffold: (I) 10-15 µm (liquid nitrogen, immersion rate: 5 $mm.min^{-1}$); (II) 30-40 µm (liquid nitrogen, 80 immersion rate: 1 $mm.min^{-1}$); (III) 60-70 µm (dry ice/acetone, immersion rate: 1 $mm.min^{-1}$); and (IV) 80-100 µm (ice/NaCl, immersion rate: 1 $mm.min^{-1}$). Once frozen, the samples were freeze-dried for 48 h (100 mTorr). The obtained ultra-lightweight monoliths retained both the size and shape of the employed moulds. The total porosity of each sample was kept constant (~ 90%), which was controlled with the amount of water in the initial dispersions. For future treatments, samples were cut into pieces of 2.5 cm in length. Freeze-dried TiO_2 scaffolds were then used as precursors of electrically conducting supports (ITTC electrodes). For this, the scaffolds were first sintered in an air atmosphere at 1000ºC for 1.5 h (heating and cooling rates: 5ºC.min^{-1}), which led to mechanically stable ceramic pieces. Electrically conducting Ti_4O_7 porous supports were then obtained from sintered TiO_2 monoliths after being reduced by elemental Zr (15 mg Zr/100mg TiO_2) at high temperature (1000ºC, 15 h) under vacuum, according to references [7] and [15]. Single phase Ti_4O_7 porous supports were finally used as electrodes to grow *G. sulfurreducens* bacteria under controlled experimental conditions. A non-porous Ti_4O_7 electrode was used as a control material. This sample was prepared according to protocols reported in the reference [7].

Bacterial strain and culture medium

G. sulfurreducens strain (DM12127, DSMZ, Germany) was used as a source of electrochemically active bacteria. The strain was first anaerobically grown in stationary batch at 32ºC in an aqueous culture medium containing 30 mM KCl, 50 mM $NaHCO_3$, 9.3 mM NH_4Cl, 2.5 mM NaH_2PO_4, vitamins and trace minerals, according to reported protocols.[16,17] Prior to inoculation in the electrochemical cells, bacteria were cultured for three weeks in fumarate-containing (40 mM) growth medium (fumarate used as electron acceptor) supplied with acetate (20 mM) used as the carbon source (electron donor).

ITTC electrode cell assembly and microbial growing protocols

Conducting supports (porous and non-porous) were separately set in three-electrode electrochemical cells, all containing 100 mL deoxygenated culture medium (free of electron acceptors), and polarized at a constant potential of 0.2 V vs. Ag/AgCl (3M NaCl) reference electrode. Electrical contact to the external circuit was performed by gluing graphite rods on the electrodes, using conducting epoxy adhesive. Graphite rods were prevented from coming into contact with the liquid culture medium. In order to continuously supply fresh medium through the oriented pores of the electrodes, a flow-through system was developed. For this, the graphite bar used to make the external electrical contact was drilled, and a rubber hose (1.5 mm internal diameter) was place in it. A peristaltic pump was used to inject culture medium (free of electron acceptors/free of planktonic cells) through the oriented electrode architectures, at a rate of 0.6 mL.min^{-1}. The reactors and all liquid reservoirs were maintained at 32ºC while continuously flushed with a N_2:CO_2 mixture (80:20) to adjust the pH to 7.4 and to prevent oxygen contamination. Each reactor was finally inoculated (through an inlet lateral port, not through the electrode pores) with 5 mL of stationary batch culture medium (containing *G. sulfurreducens* cells at a density of $2x10^5$ bacteria/mL), to allow for bacterial growth and proliferation in the polarized platforms. The reactors were first left in batch mode for 5 days until current production (20-30

View Article Online
DOI: 10.1039/C8TA02793E

μA) and stabilization were observed, after which the systems were turned into a continuous flow-through mode. See the Fig. S2 (ESI) for a schematic diagram of the experimental set-up.

Microbiological counting procedures

After one and a half months under operational conditions (and at maximum volumetric current densities), the bio-anodes were removed from the electrochemical cells to determine the microbial respiratory response on each electrode. For this, the maximum current values were related to the total number of bacteria, which was determined by isolating total microbial genomic DNA according to the phenol/chloroform method.[18] Extracted DNA was spectrophotometrically quantified (λ: 260 nm), and its purity (absence of protein contamination) assessed through the 260/280 nm absorbance ratio. The total number of bacteria was calculated from DNA concentrations based on a calibration curve. Bacterial respiratory efficiencies, expressed as current per bacterium, were determined for each electrode both at maximum current values (steady-state conditions) and at different stages during microbial evolution.

Characterizations

Electrode structural characteristics were assessed by scanning electron microscopy (SEM, Jeol JSM-6460 LV) on metal-sputtered samples. Microbial proliferation in the conducting scaffolds (porous and non-porous) was also evaluated by SEM. For this, bacteria were fixed in glutaraldehyde (2.5 wt%) for 60 min, followed by dehydration for 10 min in alcoholic solutions of increasing concentration (20, 40, 60, 80 and 100 % v/v ethanol). Thus-prepared samples were air-dried, sectioned and sputtered for microscopy observations.

Total electrode porosities were determined from bulk densities, calculated from the weight and geometrical volume of each bio-anode. Porosity (ε%) was then determined as $[1-(\delta_c/\delta_r)] \times 100$, where δ_c is the calculated density of each electrode (A: 0.45 g.cm^{-3}, B: 0.42 g.cm^{-3}, C: 0.46 g.cm^{-3} and D: 0.43 g.cm^{-3}), and δ_r is the reported density for Ti_4O_7 (4.32 g.cm^{-3}).[15]

Electrochemical determination of electrode relative surface areas was performed through capacitive current measurements. For this, bio-anodes were first immersed (the same geometrical volume) in culture medium in electrochemical reactors (in the absence of bacteria), letting them under open circuit potential (OCP) conditions for 10 h until potential stabilization. In this situation, charge was accumulated at the electrode surface/solution interface. Once stabilized, bio-anodes were set at +0.4V respect to their stabilized OCP, producing a measurable electrical current in time (Fig. S3 (A), ESI). From this information, the bio-anode relative surface areas were determined (Fig. S3 (B), ESI).

Bio-electrochemical assays were performed in three-electrode half-cells, as described in *ITTC electrode cell assembly and microbial growing protocols*. Porous bio-anodes (working electrodes) were polarized at a constant potential (0.2 V) vs. Ag/AgCl (3 M NaCl) reference electrode, employing a Pt wire as the counter-electrode. Tests were performed using a PGSTAT 101 potentiostat, controlled by the NOVA 1.6 software. The production of current was followed in time by means of chronoamperometric measurements, acquiring 1 point per minute. Volumetric current densities (shown in Fig. 2) are depicted as mean values (and their corresponding standard deviation), obtained from three independent tests conducted under the same experimental conditions. Accordingly, for each electrode, three measurements of current were taken (one from each individual reactor, according to the procedures described in *ITTC electrode cell assembly and microbial growing protocols*) and then averaged. Maximum volumetric current densities were calculated according to the geometrical dimensions of the electrodes immersed into the culture medium (cylinders of 1 cm diameter and 1.05 cm height, except for anode B that was immersed 0.86 cm) and maximum averaged currents (arrows in Fig. 3). Current densities normalized per projected surface areas were also calculated on maximum currents, but considering the projected base of the cylindrical electrodes (0.785 cm^2).

Results and discussion

Fig. 1 shows structural features (both schematic and real) of the 3D layered bio-anodes.

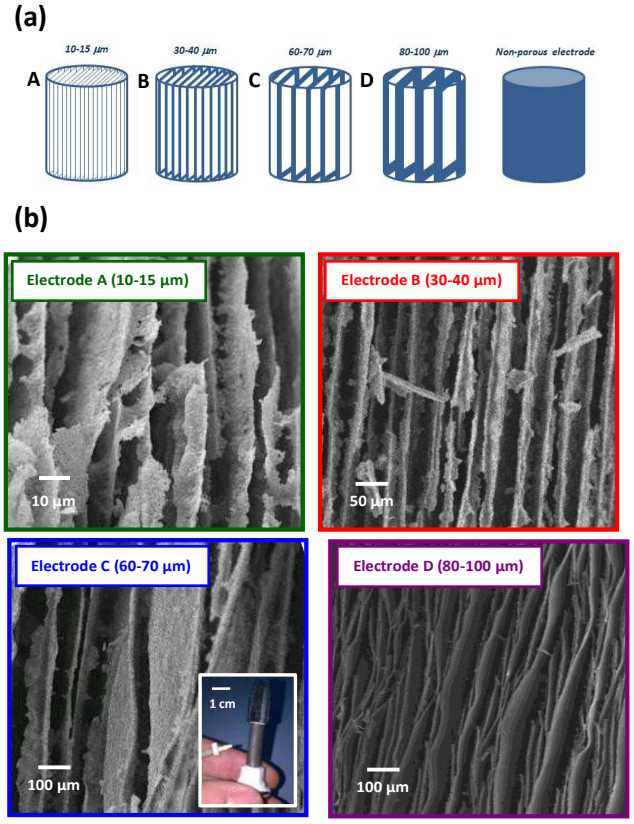

Fig. 1 (a) Schematics of the ITTC electrodes. The layered-like pore configurations represent the tested idea, which is to selectively distribute a constant porosity (90%) into slit-shaped pores with different layer-to-layer spacing: (A) 10-15 μm, (B) 30-40 μm, (C) 60-70 μm, and (D) 80-100 μm. A non-porous electrode was used for comparative purposes. Electrode geometrical dimensions: 1 cm diameter, 2 cm height. **(b)** SEM micrographs of the ITTC electrodes. The architectures consisted of aligned layers extended along of the entire electrode volume, according to the employed freezing technique. The experimental conditions used to build-up the electrode scaffolds are those depicted in Fig. S1 in the ESI. The inset picture shows the anode C mounted on a graphite tube, used to make the external electrical contact. Left on this photograph, the rubber hose and plastic connection used to flow culture medium through the oriented electrode structures. Bars: (A) 10 μm, (B) 50 μm, (C) and (D) 100 μm. See Fig. S4 in the ESI for SEM micrographs obtained at lower magnification.

View Article Online
DOI: 10.1039/C8TA02793E

The rate of heterogeneous electrochemical reactions strongly depends on the effective electrode area, which in the case of 3D porous electrodes with a fixed porosity is inversely related to the pore size. In order to have a relative quantification of the effective area corresponding to each of the ITTC platforms, we performed capacitive current measurements. As shown in Fig. S3 (ESI), taking a non-porous material as a reference, a 9-fold increase in effective area can be obtained by structuring lamellar electrodes with interlayer distances of, for instance, 60-70 µm; while a further increase to more than 30 times is reached when shorter distances between layers are set (10-15 µm). This, in theory, should boost any electrochemical reactions in the same proportions. Following this goal, 3D porous bio-anodes have been so far developed with increasingly higher surface areas, envisioning a concomitant increase in the microbial population.[9,19-21]

Under ideal conditions, the growth of *Geobacter* on a non-porous conductive material (e.g. graphite plates) leads, after about 150 hours, to the development of a biofilm of 50-60 µm in thickness that produces a current density ranging between 8-15 A.m^{-2}.[22-25] On a dense ITTC electrode (non-porous) the performance is even higher, reaching about 20 A.m^{-2} as previously reported.[7] Beyond that time, limited conduction of the biofilm matrix results in physiological stratification and accumulation of idle cells in the upper layers of the biofilm that do not contribute to current.[16,26] In order to optimize the use of these biofilms for microbial energy conversion, and taking into account that acetate oxidation, as the overall anode reaction, depends on the amount and activity of participating bacteria, the leading goal of this study was increasing the density of fully active microbes per electrode unit volume, while simultaneously analyzing the variables affecting bacterial colonization. By using the ITTC configurations for electrochemically cultivating *G. sulfurreducens*, we obtained the results shown in Fig. 2.

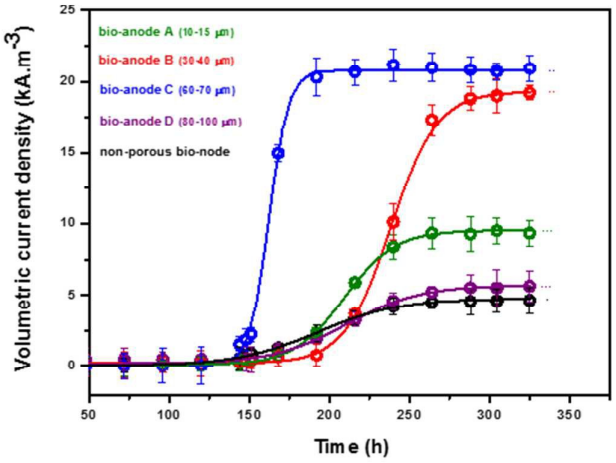

Fig. 2 Evolution of volumetric current density as a function of time. The profiles illustrate the growth and electro-catalytic activity of *G. sulfurreducens* biofilms on each bio-anode. For clarity, only the first 300 h of growing are shown. Current densities are depicted as mean values (and their standard deviation) obtained from three independent tests conducted under the same experimental conditions.

Current density output from each electrode increased by following the typical sigmoidal curve, but contrary to the dominant paradigm, maximum current densities were not obtained from electrodes with the highest specific area. In place, electrodes B and C, exhibiting intermediate layer-to-layer distances and, accordingly, intermediate electrochemical effective areas (Fig. S3 (B), ESI), were those with the best performances; producing about 18.7 ± 1.3 kA.m^{-3} (162 A.m^{-2}, normalized per projected electrode surface area) and 20.2 ± 0.8 kA.m^{-3} (213 A.m^{-2}), respectively (standard deviations refer to final current densities, which correspond to one and a half months of testing). Despite differences found among the electrodes, the electron transfer rate calculated on a per-cell basis was notably constant at about 0.11 pA per bacterium, with current scaling linearly with the size of the microbial population, regardless of interlayer spacing or developmental stage of the biofilm (Fig. 3).

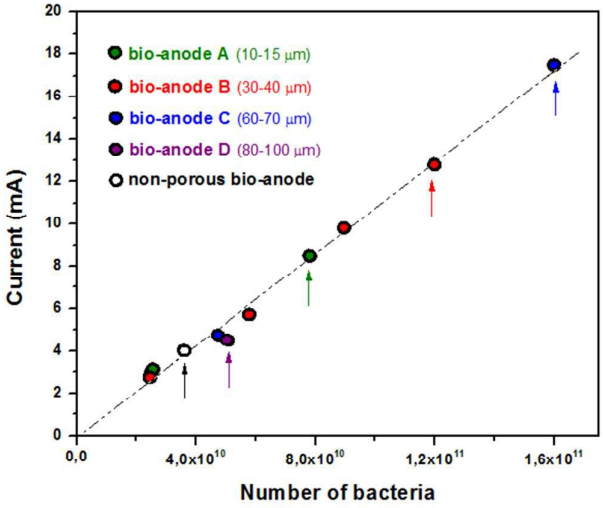

Fig. 3 Dependence of current on the number of bacteria. For each electrode, dots represent measurements at different microbial developmental stages. Arrows indicate the condition at maximum averaged currents (non-porous electrode: 3.9 mA; electrode A: 8.1 mA; electrode B: 12.75 mA; electrode C: 16.75 mA; electrode D: 4.55 mA). Maximum currents correspond to steady-state conditions. The linear trend reveals that current scales with biomass, regardless of interlayer spacing or developmental stage. According to the slope of the linear regression, an electron transfer rate of 0.11 pA per bacterium was calculated. The respiratory response equated to 228 µmol of electrons x min^{-1} x g protein^{-1} (on the basis of 0.3 x 10^{-6} µg of protein per cell of *G. sulfurreducens*).[27]

This indicates that sigmoidal curves in Fig. 2, rather than the typical growth profiles of the bacterial culture, represent the accumulation of electro-active bacteria on the electrode surface, respiring all at the same rate. This means that electrode performance is not conditioned by microbiological limitations. The calculated respiratory efficiency equates to about 230 µmol of electrons x g of proteins^{-1} x min^{-1}, well comparable to that reported on other conducting surfaces for biofilms of *G. sulfurreducens* within the critical thickness of up to 50-60 µm,[16,28-31] known to be connected by a conductive bio-matrix that warrants equivalent and maximum respiratory conditions to the whole population.

The relationship between the maximum volumetric currents presented in Fig. 2 and the relative area of each

View Article Online
DOI: 10.1039/C8TA02793E

electrode calculated in Fig. S3 (B) (ESI) is shown in Fig. 4, along with the number of bacteria accumulated in each structure.

The plot clearly shows that the overall bio-electrode performance for acetate oxidation does not depend directly on the electrode effective area, but on the amount of active bacteria supported by the electrode. Among the tested configurations, and taking into account an small layer-to-layer spacing (10-15 µm), electrode A exhibits the highest effective area per unit volume, but it can only accommodate a double amount of microorganisms as compared to the non-porous control electrode, thus leading to a maximum volumetric current density of only 9.8 ± 0.3 kA.m^{-3} (103 A.m^{-2}).

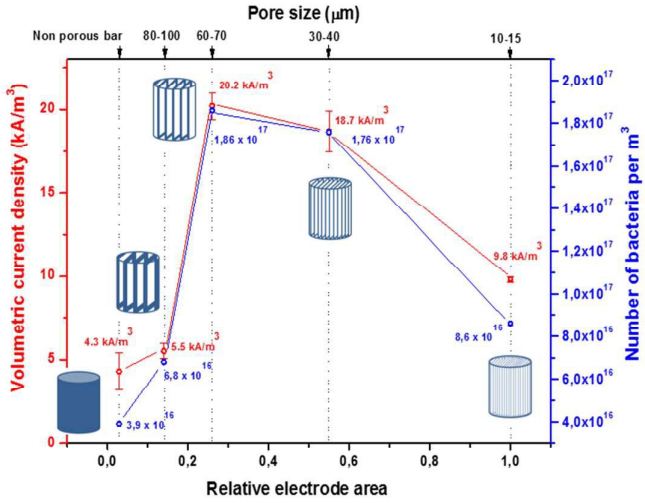

Fig. 4 Effect of layer-to-layer distance on bio-anode performance. The bell-shaped profile evidences how the anode architecture determines the maximum volumetric current density. A strong parity is observed between current and the number of bacteria accommodated on each electrode. Electrode schematics are the same as those depicted in Fig. 1a.

On the other end of the bell-shaped profile, and despite of a longer layer-to-layer distance for microbial colonization, the increase in interlayer separation up to 80-100 µm in electrode D led to a decrease in current density to 5.5 ± 0.6 kA.m^{-3} (58 A.m^{-2}), due to the low amount of bacteria that this electrode could accommodate (6.8 x 10^{16} bacteria per m^3) as a consequence, a priori, of the loss of area. Electrodes with intermediate layer spacing (B and C) clearly offered the best conditions for microbial proliferation, accommodating almost 2 x 10^{17} bacteria per m^3 and giving support to unprecedented energy conversion performances. By producing a current density over 20 ± 0.8 kA.m^{-3}, electrode C outcompetes not only ITTC electrodes with shorter or longer layer distances, but also any other single-electrode configurations reported until present days, regardless of their nature:[32] carbonaceous, oxide-based and/or metallic 3D porous electrodes (being only surpassed to date by the performance of carbonized cardboard bio-anodes;[33] although the experimental conditions used in the mentioned study cannot be exhaustively compared to ours). These results call the attention on the importance of discerning between electrochemical and bio-electrochemical effective area when optimizing bio-anodes for METs, including biocompatibility and accessibility in the definition of the latter, to ensure the area takes part effectively in the biologically mediated reaction.

Despite of the outstanding performance of electrode C, it is to note that the obtained current density represents only about 43 % of the one that could be expected by scaling the non-porous areal current density (20 A.m^{-2}) according to the effective area estimated for the electrode C (Fig. S5 in the ESI). The difference could be assigned to the reduced thickness of the biofilm found on the porous scaffold (~ 5 µm), compared to that measured on the non-porous electrode (10 µm) (Fig. S6, ESI); this indeed suggesting that electrode C could have been fully colonized. Limited thickness seems to be a common feature of biofilms growing inside porous bio-anodes,[8,9,34,35] but the reasons behind this behavior are still unknown, coming up as particularly relevant if we consider that electrode C might have yielded an unprecedented volumetric current density over 40 kA.m^{-3} by just doubling the biofilm thickness.

In the search for possible explanations for the observed limitation, the general trend presented in Fig. 4 drove the attention towards the hydrodynamic conditions developed inside the slit-shaped channels; which, despite of being known to strongly influence both biofilm development and bacterial activity, have been overlooked in precedent studies concerning electro-active bacteria confined in 3D porous electrodes. According to the flow conditions imposed in this study and the geometrical dimensions of the electrodes, a laminar-flow regime was stablished through the porous structures in the absence of bacteria. In this situation, the flow velocity profiles in the lamella-like channels are expected to follow (approximately) the analytical solution for the Poiseuille equation corresponding to parallel plates under microfluidic conditions (Fig. 5).[36] However, upon bacterial adhesion and growth, initial micro-colonies and later incipient clusters may substantially increase the flow complexity in the micro-channels by diverting liquid around biomass, thus generating flow velocity components in directions other than the primary flow direction.[36-38]

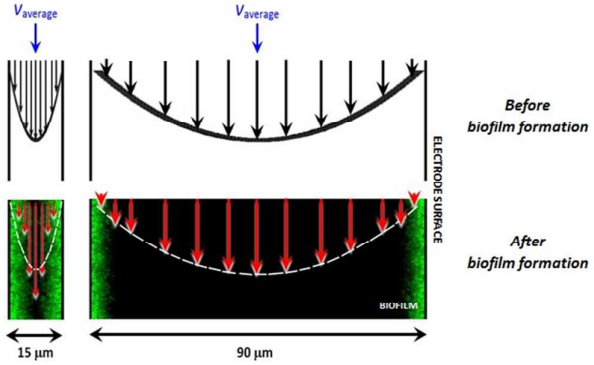

Fig. 5 Schematic representation of the flow velocity fields proposed to develop in the electrodes before and after biofilm growth. Electrode A (10-15 µm lamellar spacing) and electrode D (80-100 µm lamellar spacing) are represented. The average velocity is the same for each channel, according to the same flowing conditions used and the same geometrical dimensions (cross-section areas) for all the electrodes. Before biofilm formation, the parabolic velocity profiles correspond to the typical solution for the Poiseuille expression for parallel plates. After colonization, a redistribution of flow velocities inside the layered channels takes place, depending on interlayer distance. The parabolic dashed profile represents the Poiseuille-like behaviour. The red arrows represent the new flow velocity condition after biofilm growth, departing from the initial behaviour (this effect being more pronounced the shorter the interlayer distance). The distance between layers and biofilm thicknesses are drawn to scale.

View Article Online
DOI: 10.1039/C8TA02793E

Indeed, the reduction of the effective hydraulic channel cross-section as the biofilm develops leads to the decrease of fluid velocities near the biofilm surface, while increasing accordingly flow patterns away from it (towards the center of the channels). Interestingly, these effects are typically more pronounced the shorter the distance between layers, as schematically represented in Fig. 5.

The variability in local flow velocities has been demonstrated to produce critical changes in mass transport phenomena at the microscale,[39,40] as well as to induce strong shear stress effects over the biofilm surface.[36,41-43] Accordingly, shear forces may lead here to biomass detachment, while the increased transport of acetate may accelerate bacterial activity, thus opening the door to differential effects on both biofilm structure and performance according to the separation between electrode layers. Increased dragging forces on biofilms growing on electrode A may thus limit bacterial colonization and biofilm development inside the slit-shaped channels, explaining its low bio-electrochemical performance (Fig. S5, ESI). Particularly, the dragging hypothesis was supported by performing tests on electrode A under different flow conditions, revealing an inverse parity between flow velocity and maximum current densities. In addition, spatial variability in the development of the biofilm was also revealed in this electrode, with localized areas where microbial replication led to pore clogging events (Fig. 6), thus also conducting to limitations in transport through the porous structure.

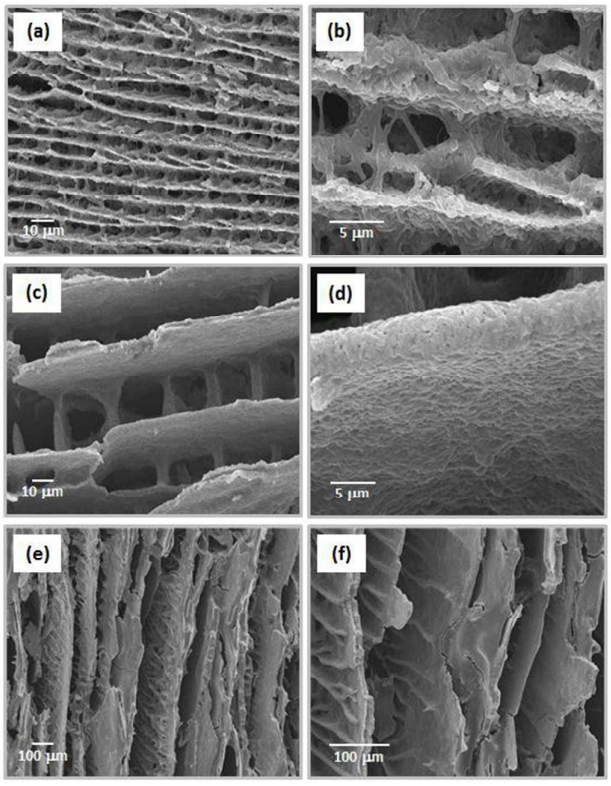

Fig. 6 Scanning electron micrographs of colonized bio-anodes: (a-b) electrode A, (c-d) electrode B, (e-f) electrode D. Unlike the general trend of tight/compact biofilms on most of the evaluated bio-anodes, electrode A evidenced less dense microbial populations, although thick enough to clog partial extensions of the porous scaffold.

This spatial heterogeneity in microbial replication may also be ascribed to a heterogeneous distribution of the electrostatic potential of the solution in contact to the anode surface, leading consequently to diverse Nernst potentials on the electrically conducting surface. This effect has been recently remarked as a possible cause for lower electrode performances and spatial heterogeneity in biofilm development for large surface area 2D bio-anodes.[44] In this way, the effect imparted by the high surface area could not reverse the combined negative features associated to the smaller pore size: both flow-induced biofilm dragging effects and pore clogging events in a highly heterogeneous microbial environment. These results knock down the paradigm towards porous bio-anodes with increasingly higher surface areas per unit volume for obtaining higher microbial colonization.

In the opposite side of interlayer spacing, we analyze electrode D. In this case, two effects may limit its performance: (i) an inherently lower surface area exposed to the microbial population (Fig. S3, ESI), and (ii) a restriction in acetate molecular diffusion across an increased mass boundary layer (MBL) inside the larger channels as a consequence of the laminar flow pattern, even in the presence of bacteria.[39,45] Additionally to the acetate transport limitation inside the pores, the mass transfer resistance also decreases the flux of waste products out of the biofilm, leading to a scenario in which local acidification due to proton production cannot be avoided (no matter the biofilm thickness). In this way, and counter-intuitively, electrodes with large-enough pore sizes could lead to detrimental effects on transport phenomena in and out of the biofilm under a flow-through configuration, especially under the laminar flow regimes developed in currently studied porous bio-anodes. Summarizing, the dynamic pattern of the culture medium flowing inside the 3D slit-shaped pores must also be playing a central role on determining the bio-anode performance, driving the attention not only to how much surface area an electrode exhibits, but also to the way in which the liquid phase behaves inside the pores according to the scenario imposed by the electrode architecture. Only the consideration and optimization of both effects, effective electrode area and flow conditions, will determine the final electrode performance.

In this framework, electrodes with intermediate surface-to-volume ratios emerge naturally as the optimum platforms to be colonized by electro-active bacteria, rendering bio-hybrid assemblies with the best yield in volumetric current density. In order to demonstrate a performance improvement framed into the state-of-the-art on the area of bio-electrochemical anodes, we set our results in context with the current literature and compare them on the basis of reported volumetric performances for true 3D monolithic porous electrodes (open macroporous platforms).

Fig. 7 depicts a bar chart with the latest reports (since 2011 onwards) on top-performance bio-electrochemical anodes. To this respect, it is worthwhile mentioning that, due to different reactor designs, diverse culture medium compositions, variable microbial inoculum sources and operational conditions, comparisons are usually difficult to put at the same level, so that exhaustive conclusions cannot be conclusively drawn. However, beyond this, and considering that current density values reported to date correspond to the best electrode performance in each study (that is, ensuring

View Article Online
DOI: 10.1039/C8TA02793E

maximum current density output), we believe this approach may be used to put our work on the table of discussion, envisioning new studies to keep increasing the bio-electrochemical anode performance.

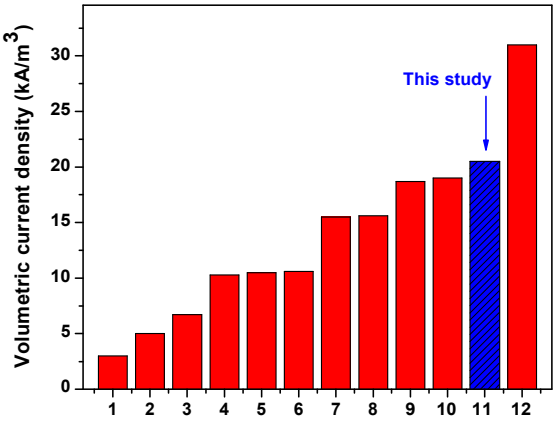

Fig. 7 Bar chart on 3D monolithic bio-anode performance. Numbers (1) to (12) correspond to different porous electrodes: (1) graphene sponge,[46] (2) graphene/PANI foam,[47] (3) graphite/PHBV (poly(3- hydroxybutyrate-co-3-hydroxyvalerate),[48] (4) RVC/CNTs,[9] (5) carbonized king mushroom,[49] (6) CNT sponge,[50] (7) copper/melamine foams,[51] (8) carbonized corn stem,[49] (9) carbonized pomelo peel,[10] (10) MWCNT/chitosan,[8] (11) macroporous Ti_4O_7 ceramics (this study), (12) carbonized corrugated cardboard.[33]

On this sense, we strongly believe that collective efforts will finally lead to the goal of improving functional electrodes for METs applications.

Conclusions

The critical improvement for obtaining the results presented here relied on controlling the layer-to-layer distance of 3D lamellar conducting scaffolds. This allowed building electrodes with slit-shaped pores with an interlayer separation between 60 and 80 µm, which provided the optimal balance between fluid dynamic conditions and bio-electrochemically effective surface areas. This combination allowed supporting the growth of an electro-active bacterial population (*G. sulfurreducens*) to a density of 1.86 x 10^{17} cells per m^3 (Fig. 4) with maximized catalytic performance (Fig. 3). In a more general view, our results indicate that maximizing the area may lead to lower performances if the density of active bacteria is not taken into account at the time of designing bio-anodes for improving METs. Indeed, they indicate that up to 75% of the total electrode area per unit volume can be effectively removed, the loss in conducting surface being counterbalanced by the improvement in the hydrodynamic conditions that favour bacterial growth. In this scenario, the concept of modulating the surface-to-volume ratio of lamellar electrodes by tuning the interlayer spacing has emerged as the cornerstone to approach to the bio-electrode architecture with the best volumetric outcome. We hope this may represent a platform towards tailored scaffolding for microbial energy transduction.

Conflicts of interest

There are no conflicts to declare.

Acknowledgements

This study has received funding from the European Union´s Horizon 2020 research and innovation program under grant agreement Nº 642190. The financial support of the National Research Council (CONICET, Argentina) and the National Agency for the Promotion of Science and Technology (ANPCyT, Argentina) is gratefully acknowledged.

Notes and references

1 K. Rabaey, L. Angenent, U. Schröder, and J. Keller (Eds.), *Bioelectrochemical systems: from extracellular electron transfer to biotechnological application*, IWA Publishing 2010.
2 M. Baca, S. Singh, M. Gebinoga, F. Weise, G. Schlingloff and A. Schober, *Adv. Energy Mater.*, 2016, **6**, 1600690.
3 S. Chu, Y. Cui and N. Liu, *Nature Mater.*, 2017, **16**, 16.
4 H. Liu, S. Cheng, S. and B. E. Logan, *Environ. Sci. Technol.*, 2005, **39**, 658.
5 L. M. Tender, S. A. Gray, E. Groveman, D. A. Lowy, P. Kauffman, J. Melhado, R. C. Tyce, D. Flynn, R. Petrecca and J. Dobarro, *J. Power Sources*, 2008, **179**, 571.
6 I. A. Ieorpoulos, A. Stinchcombe, I. Gajda, S. Forbes, I. Merino-Jimenez, G. Pasternak, D. Sanchez-Herranz and J. Greenman, *Environ. Sci.: Water Res. Technol.*, 2016, 2, 336.
7 D. Massazza, R. Parra, J. P. Busalmen and H. Romeo, *Energy Environ. Sci.*, 2015, **8**, 2707.
8 K. Katuri, M. L. Ferrer, M. C. Gutiérrez, R. Jiménez, F. del Monte and D. Leech, *Energy Environ. Sci.*, 2011, **4**, 4201.
9 V. Flexer, J. Chen, B. C. Donose, P. Sherrell, G. C. Wallace and J. Keller, *Energy Environ. Sci.*, 2013, **6**, 1291.
10 S. Chen, Q. Liu, G. He, Y. Zhou, M. Hanif, X. Peng, S. Wang and H. Hou, *J. Mater. Chem.*, 2012, **22**, 18609.
11 S. You, M. Ma, W. Wang, D. Qi, X. Chen, J. Qu and N. Ren, *Adv. Energy Mater.*, 2017, **7**, 1601364.
12 L. Zou, Y. Qiao, Z-Y. Wu, X-S. Wu, J-L. Xie, S-H. Yu, J. Guo and C. M. Li, *Adv. Energy Mater.*, 2016, **6**, 1501535.
13 H. Yi, K. P. Nevin, B. C. Kim, A. E. Franks, A. Klimes, L. M. Tender and D. R. Lovley, *Biosens.Bioelectron.*, 2009, **24**, 3498.
14 D. R. Lovley and K. P. Nevin, *Curr. Opin. Biotechnol.*, 2011, **22**, 441.
15 A. Kitada, G. Hasegawa, Y. Kobayashi, K. Kanamori, K. Nakanishi and H. Kageyama, *J. Am. Chem. Soc.*, 2012, **134**, 10894.
16 G. D. Schrott, M. V. Ordoñez, L. Robuschi and J. P. Busalmen, *ChemSusChem*, 2014, **7**, 598.
17 A. Esteve-Núñez, M. Rothermich, M. Sharma and D. R. Lovley, *Environ. Microbiol.*, 2005, **7**, 641.
18 K. Wilson, *Preparation of genomic DNA from bacteria.Current protocols in molecular biology* (1987).
19 A. P. Borole, C. Y. Hamilon, T. Vishnivetskaya, D. Leak and C. Andras, *Biochem. Eng. J.*, 2009, **48**, 71.
20 C. Zhao, P. Gai, C. Liu, X. Wang, H. Xu, J. Zhang and J-J. Zhu, *J. Mater. Chem. A*, 2013, **1**, 12587.
21 Y-Q. Wang, H-X. Huang, B. Li and W-S. Li, *J. Mater. Chem. A*, 2015, **3**, 5110.
22 C. Torres, R. Krajmalnik-Brown, P. Parameswaran, A. K. Marcus, G. Wanger, Y. A. Gorby and B. E. Rittmann, *Environ. Sci. Technol.*, 2009, **43**, 9519.
23 X. Zhu, M. D. Yates, M. C. Hatzell, H. A. Rao, P. E. Saikaly and B. Logan, *Environ. Sci. Technol.*, 2014, **48**, 1352.
24 P. S. Jana, K. Katuri, P. Kavanagh, A. Kumar and D. Leech, *Phys.Chem.Chem.Phys.*, 2014, **16**, 9039.
25 A. K. Marcus, C. I. Torres and B. E. Rittmann, *Bioresour.Technol.*, 2011, **102**, 253.
26 L. Robuschi, J. P. Tomba, G. D. Schrott, P. S. Bonanni, P. M. Desimone and J. P. Busalmen, *Angew. Chem. Int. Ed.*, 2013, **52**, 925.

View Article Online
DOI: 10.1039/C8TA02793E

27 E. Marsili, J. Sun and D. R. Bond, *Electroanalysis,* 2010, **22**, 865.
28 D. R. Bond and D. R. Lovley, *Appl. Environ. Microbiol.*, 2003, **69**, 1548.
29 G. Reguera, K. P. Nevin, J. S. Nicoll, S. F. Covalla, T. L. Woodard and D. R. Lovley, *Appl. Environ. Microbiol.*, 2006, **72**, 7345.
30 S. Ishii, K. Watanabe, S. Yabuki, B. E. Logan and Y. Sekiguchi, *Appl. Environ. Microbiol.*, 2008, **74**, 7348.
31 H. Richter, K. McCarthy, K. P. Nevin, J. P. Johnson, V. M. Rotello and D. R. Lovley, *Langmuir*, 2008, **24**, 4376.
32 X. Xie, C. Criddle and Y. Cui, *Energy Environ. Sci.*, 2015, **8**, 3418.
33 S. Chen, G. He, Q. Liu, F. Harnisch, Y. Zhou, Y. Chen, M. Hanif, S. Wang, X. Peng, H. Hou and U. Schröder, *Energy Environ. Sci.*, 2012, **5**, 9769.
34 K. P. Nevin, H. Richter, S. F. Covalla, J. P. Johnson, T. L. Woodard, A. L. Orloff, H. Jia, M. Zhang and D. R. Lovley, *Environ. Microbiol.*, 2008, **10**, 2505.
35 X. Liu, X. Du, X. Wang, N. Li, P. Xu and Y. Ding, *Biosens. Bioelectron.*, 2013, **41**, 848.
36 L. J. Song, K. H. Au, K. T. Huynh and A. I. Packman, *Biotechnol. Bioeng.*, 2013, **111**, 597.
37 J. Kim, H-S. Kim, S. Han, J-Y. Lee, J-E. Oh, S. Chung and H-D. Park, *Lab Chip*, 2013, **13**, 1846.
38 J. A. Hornemann, S. L. Codd, R. J. Fell, P. S. Stewart and J. D. Seymour, *Biotechnol. Bioeng.*, 2009, **103**, 353.
39 C. Picioreanu, M. C. M. van Loosdrecht and J. J. Heijnen, *Biotechnol. Bioeng.*, 2000, **69**, 504.
40 D. de Beer and P. Stoodley, *Water Sci. Technol.*, 1995, **32**, 11.
41 Y. C. Choi and E. Morgenroth, *Water Sci. Technol.*, 2003, **47**, 69.
42 P. Stoodley, J. D. Boyle and H. M. Lapping-Scott, *Influence of flow on the structure of bacterial biofilms. Microbial Biosystems: New Frontiers, Proceedings of the 8th International Symposium on Microbial Ecology.* Atlantic Canada Society of Microbial Ecology, 85 Halifax, Canada (1999).
43 W. Zhang, T. S. Sileika, C. Chen, Y. Liu, J. Lee and A. I. Packman, *Biotechnol. Bioeng.*, 2011, **108**, 2571.
44 M. Oliot, P. Chong, B. Erable and A. Bergel, *Chem. Eng. Sci.*, 2017, DOI: 10.1016/j.cej.2017.06.044
45 P. Stewart, *Biofouling*, 2012, **28**, 187.
46 W. Chen, Y-X. Huang, D-B. Li, H-Q. Yu and L. Yan, *RSC Adv.*, 2014, **4**, 21619.
47 Y-C. Yong, X-C. Dong, M. B. Chan-Park, H. Song and P. Chen, *ACS Nano*, 2012, **6**, 2394.
48 H. R. Luckarift, S. R. Sizemore, K. E. Farrington, J. Roy, C. Lau, P. B. Atanassov and G. R. Johnson, *ACS Appl. Mater. Interfaces*, 2012, **4**, 2082.
49 R. Karthikeyan, B. Wang, J. Xuan, J. W. C. Wong, P. K. H. Lee and M. K. H. Leung, *Electrochim. Acta*, 2015, **157**, 314.
50 X. Xie, M. Ye, L. Hu, N. Liu, J. R. McDonough, W. Chen, H. N. Alshareef, C. S. Criddle and Y. Cui, *Energy Environ. Sci.*, 2012, **5**, 5265.
51 A. Baudler, M. Langner, C. Rohr, A. Greiner and U. Schröder, *ChemSusChem*, 2017, **10**, 253.